Garnet–olivine equilibration during cooling in the mantle

Douglas Smith and Clark R. Wilson

Department of Geological Sciences
University of Texas, Austin, Texas 78712

Abstract

Garnet–olivine equilibration during cooling has been modelled with numerical experiments which simulate Fe–Mg exchange and diffusion in radially-symmetric arrangements of olivine and garnet. Calculated compositional profiles in garnet become zoned in Fe and Mg for cooling histories plausible for the mantle. For the most reasonable diffusion parameters, zoning starts to occur at temperatures below 800°C and continues to develop over a cooling range of about 200°C. Strong zoning in garnet is confined to within 1000 μm of olivine–garnet contacts. During the simulated cooling, small olivine inclusions in garnet become more magnesian than larger ones.

Electron microprobe studies of inclusions from diatremes have been compared to the results of the numerical experiments. Garnet fragments from Colorado Plateau diatremes have radial Fe–Mg zoning about olivine inclusions, and compositions of these olivine inclusions depend upon their size. Calculated temperatures for the olivine–garnet pairs are near 550°C. Garnets in three nodules from the Jagersfontein kimberlite pipe are not Fe–Mg zoned in contact with olivine, and calculated temperatures for the three nodules are 700–800°C. Our observations and calculations are consistent with the hypothesis that olivine and garnet in the mantle equilibrate to temperatures near 700°C. Pyroxene and garnet appear to equilibrate to similar temperatures during slow mantle cooling. The apparent paucity of low-temperature garnet lherzolite nodules in diatremes is unlikely to be due either to the miscalibration of geothermometers or to olivine–garnet disequilibrium.

Introduction

Temperatures and pressures calculated for garnet peridotite nodules may reflect the ambient conditions at the depth from which the nodules were sampled (e.g., Finnerty and Boyd, 1984). On the basis of diffusion data, however, Harte and Freer (1982) suggested that some peridotite phases might cease to equilibrate below about 900°C during cooling in the mantle, though olivine and garnet might remain in Fe–Mg exchange equilibrium to lower temperatures. If so, then calculated temperatures for some nodules might be based on cation distributions quenched in during cooling in the mantle, and the calculated values would not represent conditions from which the nodules were erupted. Also, some of the differences between results of different geothermometers could reflect diffusion kinetics. Support for these ideas comes from many demonstrations of major element and isotopic disequilibria in spinel peridotite nodules (e.g., Smith and Levy, 1976; Hofmann and Hart, 1978) and granulite inclusions (Harte et al., 1981). Moreover, very few garnet peridotite nodules collected from diatremes have calculated equilibration temperatures below 800°C. Garnet peridotite should be stable to lower temperatures in cool subcontinental mantle, however, since the low-tempera-

ture transition from spinel to garnet peridotite occurs at about 16 kbar for Cr-free peridotite and at slightly higher pressures for the Cr-poor spinel lherzolite nodules typically found in volcanic rocks (O'Neill, 1981). These pressures should be exceeded at temperatures above 600°C in shield areas with heat flow values near 40 mW/m^2 (Pollack and Chapman, 1977). The paucity of calculated temperatures below 800°C is readily explained, however, if equilibria typically freeze for garnet peridotite phases near or above this value. If blocking temperatures for common geothermometers exceed 800°C, the lower-temperature parts of mantle geotherms like the one proposed by Boyd (1973) could reflect kinetics of mineral equilibration rather than actual variations of temperature with depth, as suggested by Harte and Freer (1982).

We have investigated the behavior of garnet peridotite equilibria during cooling in the mantle by making numerical experiments and by analyzing unusually low-temperature inclusions from diatremes. The numerical experiments simulate Fe–Mg exchange and diffusion during cooling of olivine–garnet pairs. Plausible mantle cooling histories and a range of diffusion rates are used in the models. Fe–Mg zoning is produced in garnet during simulated cooling below the temperatures at which equilibrium is maintained. We have compared the calculated

zoning and model temperatures with data on inclusions from diatremes on the Colorado Plateau and from the Jagersfontein kimberlite pipe in South Africa. The comparison not only helps to establish the conditions at which cation distributions are frozen in during mantle cooling, but it also bears on the validity of extrapolated diffusion rates and on olivine–garnet geothermometry at low temperatures.

Numerical model

General description

The distribution of Fe and Mg between coexisting olivine and garnet is dependent upon temperature, pressure, and composition. If the two phases are initially at equilibrium and then cooled, Fe and Mg exchange will proceed at mutual contacts, and interdiffusion of the cations will take place away from the interfaces. Although analytical methods for characterizing the compositional gradients resulting from such a process have been developed (Lasaga et al., 1977; Lasaga, 1983), realistic geometries and thermal histories are best treated numerically. Onorato et al. (1981) and Sanford (1982) have described numerical techniques for investigating the problem. Wilson (1982) and Ozawa (1983) have discussed models similar to ours and applied them to olivine–spinel pairs.

Our numerical model treats spherically-symmetric arrangements; most calculations were done for an olivine matrix about a garnet crystal with a small central inclusion of olivine. Garnet–olivine compositions were held in equilibrium at mutual interfaces by Fe–Mg exchange, using a temperature-dependent distribution ratio, as discussed below. Fluxes were balanced at each interior interface and held at zero at the outer perimeter of the volume. Interface positions were fixed during cooling, as volume changes during Fe–Mg interdiffusion were presumed negligible. The numerical solution of the diffusion equation in the radial coordinate was accomplished using a backward time-difference algorithm. At the onset of cooling, the phases were homogeneous and in mutual equilibrium. Cooling was usually accomplished in a thousand or so time steps; the lengths of the time steps were increased during the cooling process. Solutions showed no significant changes when more steps were used. Further details of the procedure are discussed by Wilson and Smith (1984b), and equations are briefly summarized in an appendix to this paper.

Exchange and diffusion parameters

Two independent calibrations are available for the garnet–olivine geothermometer, and the distribution coefficient for Fe and Mg at garnet–olivine interfaces, K_D (Fe/Mg in garnet divided by Fe/Mg in olivine), can be calculated from each one. The calibration of O'Neill and Wood (1979) was based upon experiments at temperatures from 900 to 1400°C, while that of Kawasaki (1979) was based upon experiments in the range 1000–1300°C. To use either calibration in our models, the distribution coefficient must be extrapolated to temperatures well below the experimental control, and olivine compositions, pressures, and Ca/(Ca+Fe+Mg) values in garnet must be specified. Calculated values of K_D by the two methods are similar except at temperatures below 650°C, where the Kawasaki-based algorithms yield appreciably larger values (Fig. 1) which are unreasonably sensitive to olivine composition. Since the
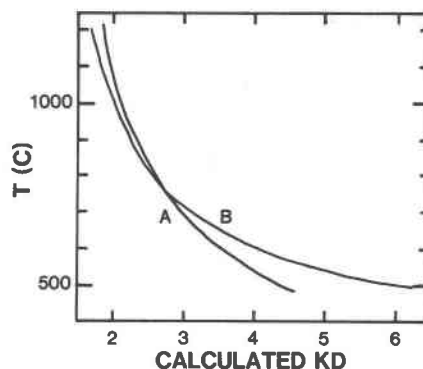

Fig. 1. Dependence of K_D (Fe/Mg in garnet divided by Fe/Mg in olivine) upon temperature, as calculated from the algorithms of O'Neill and Wood (1979) (Curve A) and of Kawasaki (1979) (Curve B). K_D values were calculated for olivine with 6 mole percent fayalite, garnet with Ca/(Ca+Fe+Mg) of 0.137 and a pressure of 25 kbar.

O'Neill–Wood formulation in part is based upon lower-temperature experiments, and since it is less sensitive to compositional variations at low temperatures, it was used to calculate a temperature dependence for K_D in our numerical experiments. We expressed that dependence as

$$\frac{\partial(\ln K_D)}{\partial T}\Bigg]_P = \frac{-H}{RT^2}$$

where H = 12150 /mole, a value appropriate for olivine with 6 mole% fayalite, garnet with Ca/(Ca+Fe+Mg) = 0.137, and a pressure of about 25 kbar. Although the mineral compositions were chosen specifically for Colorado Plateau pairs, they are reasonable for many garnet peridotites.

Interdiffusion rates for Fe and Mg in olivine are relatively well-known, based upon the experimental studies of Buening and Buseck (1973) and of Misener (1974). These workers determined rates as functions of crystallographic direction, oxygen fugacity, olivine composition, and pressure at temperatures above 900°C. Buening and Buseck fit their data to different parameters above and below 1125°C; their data illustrate the danger of extrapolating diffusion coefficients over a large temperature range assuming the same temperature dependence. When the different oxygen fugacities of experiments are taken into account, the extrapolated results of Buening and Buseck (1973) are about an order of magnitude greater than those of Misener (1974) over the temperature range 1100–500°C. This degree of uncertainty has little effect on the calculations of garnet zoning, since diffusion rates in garnet are so much slower than those in olivine. Lasaga et al. (1977) showed that when diffusion rates are much faster in one of two phases, zoning profiles in the other are relatively insensitive to uncertainties in the faster rate. A pre-exponential term of 1.557×10^{-7} m²/sec and an activation energy of 203470 j/mole have been adopted for olivine in our model, consistent with extrapolation of the data of Buening and Buseck (1973) to oxygen fugacities of the FMQ buffer.

Experimental studies of Fe–Mg interdiffusion rates in garnet have been reported in four sources (A—Freer, 1981; B—Duckworth and Freer, 1981; C—Elphick et al., 1981; D—Cygan and Lasaga, 1983), and some of the experimental conditions and derived parameters are summarized in Table 1. The differences

Table 1. Fe–Mg interdiffusion in garnet

D (m*m/sec)	Q (j/mole)	Source and Comments	Data Set
$6.11 * 10^{-4}$	344000	Freer (1981) from work progress by Duckworth and Freer: 1150-1330°C at 30 kb	A
$5 * 10^{-10}$	208000	Duckworth and Freer (1981) for pyrope in matrix of almandine at 1050-1380°C, 30 kb	B
$2.3 * 10^{-6}$	369000	Elphick et al. (1981) at 1350-1525°C and 40 kb. Preferred values, almandine-rich garnet	C
$5.6 * 10^{-8}$	255000	Cygan and Lasaga (1983) for natural pyrope at 750-900°C, 2 kb. Stated for Mg self-diffusion	D

between the formulations may reflect the different compositions and temperature ranges studied, but none of these experiments has been described in detail. Hence, it is difficult to decide which is superior. Our numerical calculations were extended to temperatures below 600°C, and diffusion rates from the four sources extrapolated to these low temperatures do not agree (Fig. 2). Studies of zoning in garnets in crustal rocks are helpful in evaluating the accuracies of these extrapolations, but diffusion rates in iron and manganese-rich garnets in the crust may not be appropriate for magnesian garnets at the higher pressures and lower oxygen fugacities likely for the mantle. The studies of crustal rocks indicate that diffusion is fast enough to homogenize garnets above about 650°C, but slow enough to preserve zoning with little alteration below about 550°C (e.g., Tracy, 1982). The estimate of Fe–Mg diffusion in Fe-rich crustal garnet at 675°C obtained by Lasaga et al. (1977) is in best agreement with the extrapolation of the parameters of Set A (Fig. 2). The parameters

of Set D, however, were determined with the starting material and temperature range most appropriate for the rocks studied here. Since the uncertainties in diffusion rates in garnet are of particular importance, parameters of Sets A, B, and C were all used in our numerical model in order to encompass the range of extrapolated values.

Cooling histories

Calculations have been made for linear and exponential cooling and for a cooling-slab model. In the slab model, temperature decreases follow an error-function behavior appropriate for a semi-infinite slab, initially uniform in temperature, with its boundary held at a fixed temperature. The thermal diffusivity of the slab is assumed constant at 2.641×10^{-5} km²/yr, a value suggested for the upper mantle by Oldenburg (1975). The depth within the slab, the surface temperature, and the initial temperature were selected for each series of calculations. The surface temperature was commonly fixed at 500°C, a plausible value for the base of the crust in a stable continental environment: the model offers a simple approximation to temperature decline in the mantle after orogeny or after continental delamination like that suggested by Bird (1979). Experiments in which the temperature decayed linearly were used to examine the effects of different cooling rates upon zoning. These experiments showed that the zoning changed only slightly for a change of an order of magnitude in cooling rate, at mantle temperatures. Thus, more complicated cooling models, as might better describe mantle diapirs of limited size, are not expected to yield results much different from those obtained here.

Calculated compositional profiles

Most numerical model calculations were made for a central olivine sphere (230 μm radius) surrounded by a garnet shell (3500 μm outer radius) surrounded by olivine to the perimeter at 8000 μm. Garnet occupies about 8% of this total volume, a percentage similar to that in many garnet lherzolite nodules. Cooling was begun at 1200°C, with an initial olivine composition of 8 mole% fayalite.

Olivine zoning was negligible, even for very rapid cooling. For example, after a calculated cooling from 1200 to 600°C at a linear rate of 1000°C per million years (with the diffusion parameters of Set A in Table 1), the interior olivine sphere was constant in composition to four significant figures; the outer olivine shell varied only from 7.82 mole% fayalite at 3510 μm to 7.85 percent at the perimeter (8000 μm). Olivine zoning is thus ignored in subsequent discussions of calculated profiles.

Compositional profiles in a garnet at four temperatures from one numerical experiment are shown in Figure 3. The experiment simulates conditions 20 km below the 500°C surface of a conductively cooling slab, initially at 1200°C; the diffusion parameters of Set A in Table 1 were used. The garnet is reequilibrated and is unzoned at 900°C, although model cooling from 1200°C took only 12 million years. Zoning appears below 800°C and is obvious by 700°C, after 56 million years total time. After 234 million years, the garnet is at 600°C, and zoning is pronounced in the outer 1000 μm. Following an additional
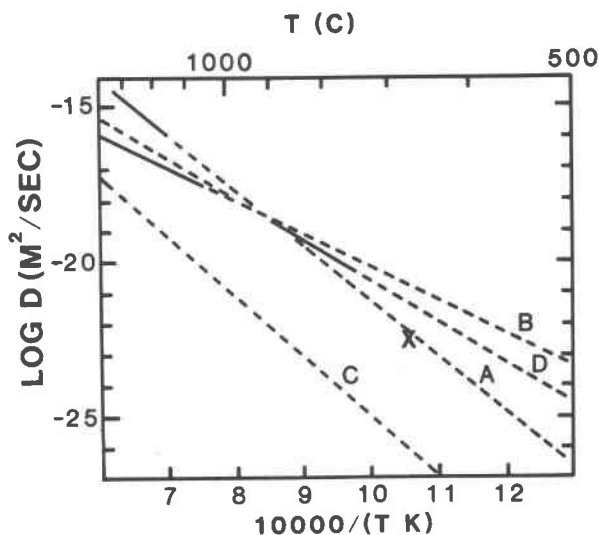

Fig. 2. Lines show the calculated diffusion coefficients as functions of temperature, according to the four sources discussed in Table 1. The solid portions of the lines show the temperature ranges of the experimental studies. The "X" shows an estimate of Lasaga et al. (1977) for a crustal garnet.
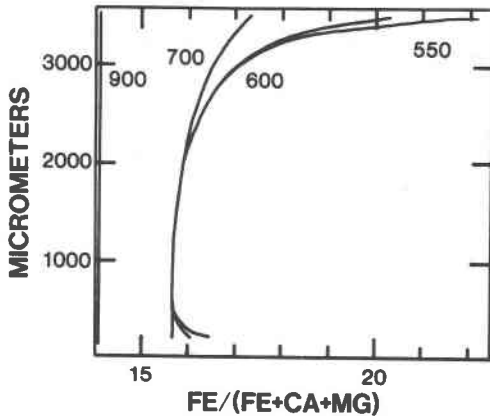
Fig. 3. Calculated compositional profiles in garnet for a cooling history beginning at 1200°C in a slab with a surface temperature of 500°C and with the diffusion parameters of Set A. The garnet extends from a central olivine inclusion (radius 230 μm) to the outer olivine shell which begins at 3500 μm. Profiles are shown at 900, 700, 600, and 550°C.

710 million years, more than three times the prior cooling period, the garnet is at 550°C; during this interval the zoning changes significantly only within 200 μm of the outer olivine-garnet contact and 100 μm of the inner one. Thus most characteristics of the zoning develop within an interval of about 200°C.

To illustrate the effects of different diffusion parameters for garnet, compositional profiles obtained with sets A, B, and C of Table 1 are shown in Figure 4. For thermal histories of a cooling slab (Fig. 4a), garnet zoning is produced in a different temperature range for each set of parameters. Marked zoning is produced above 900°C and little changed at lower temperatures for the slow diffusion rates of Set C, while for Set B, zoning is not marked until about 600°C and changes appreciably with cooling to below 550°C. The slab model used here is not useful for temperatures below 550°C, as temperatures approach the surface value, 500°C, very slowly; the average cooling rate from 550 to 540°C is about 1 degree per 50 million years. Linear cooling histories at one degree per million years were used to compare final profile shapes with each set of diffusion parameters. The final shapes are similar, but each profile has a different mean iron content (Fig. 4b). These different iron contents largely reflect differing amounts of iron depletion of the outer olivine reservoir at higher temperatures. No matter which set of diffusion parameters is adopted, distinct Fe–Mg zoning arises in the outer 1000 μm of the garnet.

Isothermal annealing will erase the zoning only if the annealing occurs in or above the upper part of the critical temperature range in which strong zoning originates. For instance, the effects of annealing for 500 million years at both 700 and 600°C are shown in Figure 4c, using the diffusion parameters of Set A. Although annealing at 700°C homogenizes the garnet, annealing for the same time period leaves the 600°C profile almost unaffected.
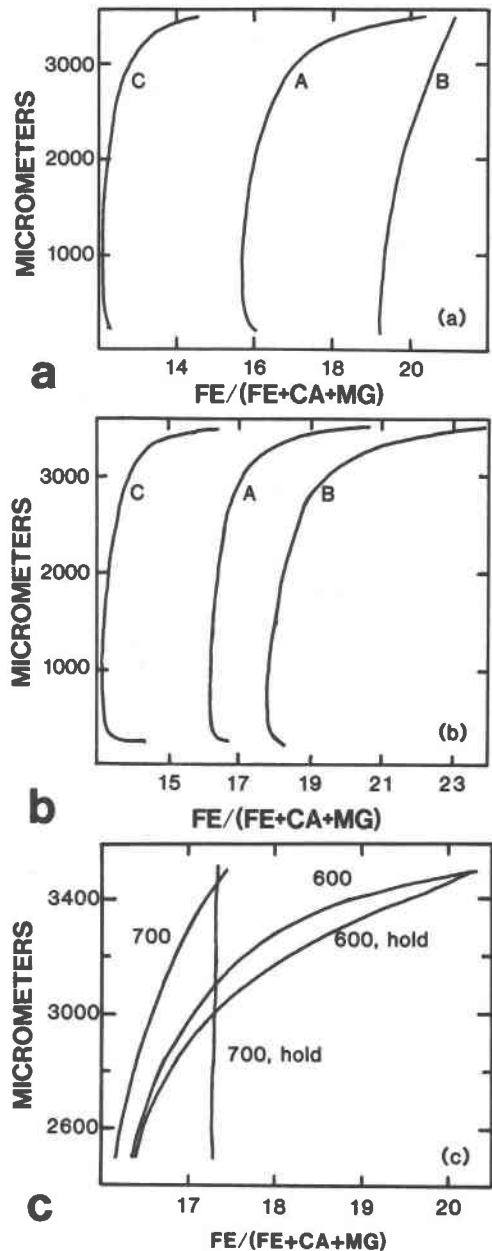

Fig. 4. Comparisons of numerical experiments with different garnet diffusion parameters and cooling histories. (A) Compositional profiles in garnet for the cooling slab model, using the diffusion parameters of Set A (at 600°C), Set B (at 550°C), and Set C (at 900°C) (B) Compositional profiles in garnet for linear cooling at 1°C per million years, using the diffusion parameters of Set A (600°C), Set B (600°C) and Set C (500°C). (C) Comparisons of compositional profiles before and after annealing at constant temperature for 500 million years. Though the model garnet was 3500 μm in radius, profiles are shown only for the outer 1000 μm. One pair of lines shows results for first cooling to 700°C and then for holding 500 million years at that temperature; homogenization is complete after the annealing time. In contrast, the profile produced after cooling to 600°C is nearly unaffected by the subsequent annealing. Profiles were calculated using the diffusion parameters of Set A.

An approximate measure of the distance over which diffusion is effective is the square root of the product of the diffusivity and time. To evaluate this quantity during cooling, values for the function

$$\left[\int_{T+100}^{T} D(t)dt \right]^{1/2}$$

were calculated numerically for a linear cooling rate of 1 degree per million years and plotted at the midpoints of the 100°C intervals. Curves drawn through the points calculated with the diffusion parameters of Sets A, B, and C are shown in Figure 5. The curves are appropriate for spherical garnets only when values are small compared to radii; otherwise, the distances for effective diffusion are underestimated. For distances greater than a few thousand μm in Figure 5, typical mantle garnets 1 cm or less in diameter would homogenize readily, and zoning would not be expected. Distances less than a few hundred μm in Figure 5 correspond to temperatures at which strong zoning can be expected, and these values occur below about 850°C (Set C), 650°C (Set A), and 550°C (Set B). The cooling rate chosen for these calculations is plausible for the upper mantle at low temperatures, but if the rate differed by a factor of 100 in any temperature interval, temperature inferences made from curves A and C would change by less than 100°C. The different effects of annealing at 600 and 700°C shown in Figure 4c can be predicted from curve A in Figure 5.

While olivine never becomes appreciably zoned, the olivine inclusion in garnet becomes more magnesian than the outer olivine shell during typical cooling histories. For instance, with a linear cooling rate of 1 degree per million years and diffusion parameters of Set A, at 700°C the compositions of inclusion and shell are 7.20 and 7.72
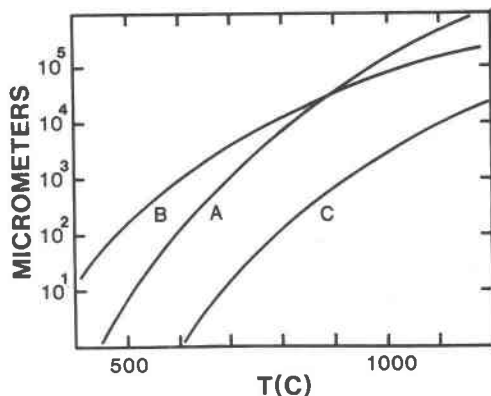
mole% fayalite, while at 500°C, compositions are 6.26 and 7.69%, respectively. The composition of the olivine inclusion at low temperatures also depends upon its size. For instance, after cooling to 500°C, the compositions of olivine inclusions of 80, 120, and 230 μm radius are 5.94, 6.05, and 6.26 mole% fayalite, respectively. These compositional differences arise in spherical geometries at temperatures low enough that the volume of garnet exchanging Fe–Mg with olivine is limited by diffusion.

Observations of low-temperature pairs

Colorado Plateau diatremes

The ultramafic diatremes of the Colorado Plateau in the southwestern United States bring up a variety of mantle fragments. Garnet peridotite nodules are extremely rare, but angular fragments of pyrope containing inclusions of olivine, diopside, and enstatite are common (McGetchin and Silver, 1970). Most individual pyrope fragments are homogeneous except for iron-enriched, magnesium-depleted zones around olivine inclusions (Hunter and Smith, 1981). Wilson and Smith (1984a) showed that the zoning profiles radial to these olivine inclusions could be fit by profiles generated using the numerical model with the diffusion parameters of Set A. They found the best fits for cooling histories which ended near 550°C. The final temperature is in agreement with results of the olivine–garnet geothermometers of Kawasaki (1979) and O'Neill and Wood (1979), which yielded temperatures of 580–600°C and 500–520°C, respectively, at 20 kbar for olivine and garnet about 5 μm from mutual contacts.

The hypothesis that the Colorado Plateau pairs cooled to low temperatures is supported by new data on the compositions of two olivine inclusions in one garnet fragment. The pyrope crystal is angular, with a maximum diameter of about 6 mm. It appears homogeneous except for Fe–Mg zoning around an olivine inclusion (Wilson and Smith, 1984a). Further polishing exposed a second olivine inclusion as well. The larger olivine inclusion, with a radius of 230 μm, contains 5.96 wt.% FeO; the other inclusion, with a radius of 150 μm contains 5.58 wt.%. The precision of these iron analyses was about 0.04 wt.% (1 sigma). Since the pyrope fragment is generally homogeneous, the compositional difference between the two olivine inclusions is best expained by the size-composition relation discussed above.

The Colorado Plateau olivine–garnet assemblages thus provide an example of low-temperature disequilibrium in the mantle. The low calculated temperatures, near 550°C, are consistent with the temperatures expected for such disequilibrium from our model results. Temperatures in the part of the mantle containing the garnets actually could have been considerably lower than the calculated temperatures, however, since the models show that zoning changes very little with further cooling. The lack of zoning at margins of the angular garnet fragments is

Fig. 5. Curves show effective diffusion distances in μm for linear cooling of 1°C per million years through 100°C intervals. Each curve is drawn through points plotted at the midpoints of 100°C intervals: the points were calculated from the square roots of the products of diffusivity and time, calculated by numerical integration over the 100°C intervals, using the diffusion parameters of Sets A, B, and C in Table 1.

probably due to the fact that they represent interior remnants of larger crystals; pronounced zoning is produced only within the outer 1000 μm of each radial profile produced in our calculations (Fig. 4).

Jagersfontein kimberlite pipe

The Jagersfontein kimberlite pipe in South Africa contains a variety of garnet peridotite nodules (Harte and Gurney, 1982). For this study, three coarse nodules with particularly low calculated temperatures and markedly different textures were selected; the initial temperature estimates were based upon preliminary electron probe studies of a large population by J. Johnson (pers. comm., by I. D. MacGregor). Harte and Gurney (1982) suggested that mineral equilibria in such nodules from Jagersfontein ". . . had probably become frozen prior to sampling by the kimberlite . . ." We looked for zoning in the minerals in the three nodules in order to evaluate the hypothesis of disequilibrium, with particular emphasis on sample J34, because it contains equant garnets up to 2 mm in radius with some unaltered margins.

Rock J34 is a garnet harzburgite with about 13% garnet, 26% orthopyroxene, a trace of diopside, and several percent amphibole. The remainder of the rock is olivine, in unstrained cyrstals up to 12 mm in diameter, and serpentine and phlogopite replacing olivine and in late veins. The amphibole occurs in equant crystals about 2 mm in diameter and in small crystals in veins with serpentine and phlogopite. The orthopyroxene crystals have only sparse exsolution lamellae. Analyses of minerals (Table 2) show compositions similar to those summarized by Harte and Gurney (1982) for Jagersfontein rocks. Analyses were by standard electron probe techniques, as

described in detail by Smith and Ehrenberg (1984): particular care was taken to assure both accurate and precise analyses of Ca and Al in orthopyroxene.

Garnet, orthopyroxene, and olivine crystals in rock J34 were analyzed at many points to search for inhomogeneities: none was found. In particular, Fe, Ca, and Mg analyses were made of garnet cores and of rims separated from contact with olivine, diopside, and orthopyroxene by minimal thicknesses of serpentine. For instance, analyses were made of garnet within about 40 and 120 μm, respectively, of bordering diopside and orthopyroxene. Analyses of points along a diameter of a garnet crystal (Fig. 6) show typical homogeneity. One end of the diameter is separated from analyzed olivine by only about 100 μm of serpentine, apparently an olivine replacement product. Similarly, no Ca, Al, Fe, or Mg zoning could be found in orthopyroxene.

Harzburgites J17 and J41 were studied in less detail. In rock J17, garnet occurs in necklace textures about orthopyroxene crystals, so the garnet probably formed by granule exsolution. The orthopyroxene crystals typically have some regions crowded with fine exsolution lamellae, and so orthopyroxene homogeneity is difficult to test. The garnet crystals, however, appeared homogeneous for all elements, including Cr, Fe, and Mg. In rock J41, garnet occurs in small subhedral crystals interstitial to much larger crystals of olivine and orthopyroxene. Some of the garnet crystals include irregular shreds of spinel, suggesting that the garnet formed at the expense of the oxide. The orthopyroxene in rock J41 has few lamellae and is homogeneous for Al, Ca, Fe, and Mg. The garnet is homogeneous for Fe and Mg but has irregular variations of Cr_2O_3 from 1.8 to 2.4 wt.%. Compositions of all phases in these rocks (Table 2) are similar to those summarized

Table 2. Mineral compositions—Jagersfontein nodules

	Ol	Opx	Cpx	Gar	Ol	Opx	Cpx	Gar	Sp	Ol	Opx	Cpx	Gar	Amph
	1	2	3	4	5	6	7	8	9	10	11	12	13	14
	J17	J17	J17	J17	J41	J41	J41	J41	J41	J34	J34	J34	J34	J34
SiO_2	41.2	57.7	54.0	41.6	41.3	57.5	54.6	42.1	na	41.0	57.2	54.3	42.3	46.7
TiO_2	na	na	na	na	na	.00	na	.02	na	na	na	na	.00	na
Al_2O_3	na	.78	2.12	21.5	na	.72	1.59	22.5	19.8	.00	.81	2.55	22.0	10.7
Cr_2O_3	na	.19	1.22	2.10	na	.16	1.01	2.39	50.8	.00	.22	1.77	2.75	2.30
Fe as FeO	7.42	4.72	1.39	8.23	7.01	4.46	1.18	8.32	16.7	7.69	4.74	1.92	8.31	2.73
MgO	52.2	36.8	17.1	20.5	51.5	36.9	17.5	19.7	13.1	51.9	36.7	16.4	20.7	20.3
CaO	.01	.21	22.7	5.18	.02	.18	23.4	5.45	.16	.01	.20	21.5	5.02	10.3
Na_2O	na	na	1.34	na	na	na	1.01	na	na	na	na	1.91	na	3.72
	100.8	100.4	99.9	99.1	99.9	99.9	100.3	100.6	100.5	100.6	99.9	100.4	101.0	97.6

na not analyzed

1-4 Rock J17, points A11, A4, A6, and A2 respectively

6-9 Rock J41, points C6, C1, C8, CC10, and A6, respectively

10-14 Rock J34, points B8, A7, A6, A1, and C4, respectively
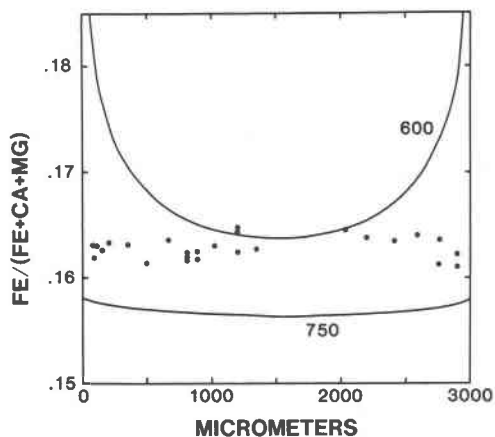
(#14 includes 0.82% K_2O)

Fig. 6. Compositional data from electron microprobe analyses along a diameter of a garnet crystal in Jagersfontein nodule J34, compared with calculated compositional profiles for a garnet of similar size. The profiles are calculated for 750 and 600°C temperatures of a linear cooling history beginning at 1100°C, using the diffusion parameters of Set A. The absolute levels of the calculated profiles are not meaningfully related to the actual garnet composition. Rather, the calculated profiles show the extent and degree of curvature expected as cation profiles are frozen in during cooling. The scatter of the duplicated compositional measurements is due to counting statistics and instrumental drift, and the scatter can be used to assess the precision with which homogeneity is defined.

Table 3. Data for pressure and temperature assignments, Jagers fontein nodules*

	J17	J34	J41
Wells, Wood T, P	772,26	808,27	769,26
Kretz (Ca in augite) T	708	795	662
Ellis-Green, Wood T, P	790,27	936,35	718,22
Kawasaki, Wood T, P	747,24	770,25	698,21
Kawasaki, 20 kb T	725	742	691
Kawasaki, 30 kb T	779	798	742
O'Neill-Wood, 20 kb T	704	727	652
O'Neill-Wood, 30 kb T	761	785	707
CaO in opx (wt. %)	.21	.20	.18
Al_2O_3 in opx (wt. %)	.78	.81	.72
Ca/(Ca+Mg)cpx	.488	.485	.490

*Calculated pressures and temperatures are in kb and °C.

for Jagersfontein coarse peridotites by Harte and Gurney (1982).

Temperatures calculated using several geothermometers for these rocks are summarized in Table 3, together with pressures based upon the method of Wood (1974). All calculated temperatures fall in the range 650–810°C, except the temperature of 936°C calculated for rock J34 by the method of Ellis and Green (1979), which is based upon the partition of ferrous iron between garnet and clinopyroxene. The mineral analyses were repeated several times with similar results, and the high garnet–clinopyroxene temperature may reflect an unusually high ferric iron content of the clinopyroxene. The two-pyroxene thermometer of Lindsley and Andersen (1983) and Lindsley (1983) is calibrated below 900°C better than any other method used here, but none of these clinopyroxenes is sufficiently low in non-quadrilateral components for proper application of the method. The temperature range from the geothermometers may simply reflect analytical errors and inaccuracies in calibration, and all three rocks could have equilibrated at identical temperatures. The insignificant range in calcium contents of orthopyroxene supports such an interpretation. The temperatures probably were in the range 700–800°C.

Discussion

The absence of Fe–Mg zoning in the Jagersfontein garnets, the calculated temperature range of 700–800°C,

and the presumption of equilibrium are consistent with cooling models using the diffusion parameters of Sets A, B, and D (Table 1). The diffusion parameters of Set C were determined at higher temperatures than the other sets: below 1000°C these parameters yield diffusion rates which are too low to be consistent with the Jagersfontein data, since numerical experiments using Set C develop zoning above 900°C.

Harte and Freer (1982) employed some of the same diffusion parameters used here to calculate times necessary for mineral equilibration in garnet peridotite phases, and our work is an extension of their approach. They concluded that ". . . the mineral compositions in many coarse nodules were frozen long before eruption, rather than being quenched in the rocks at the time of eruption." Our approach is more sensitive, since it utilizes zoning formed during cooling, rather than average distances for effective diffusion at fixed temperatures. The results of the numerical experiments show that when the interior of a garnet crystal is in pronounced Fe–Mg exchange disequilibrium with adjacent olivine due to mantle cooling, the garnet is zoned in Fe and Mg on a readily detectable scale. Typical calculated profiles are shown with microprobe data for a garnet in the low-temperature peridotite J34 in Figure 6. The precision of the data should be more than adequate for detection of zoning like that calculated for cooling to the lower temperature. Aside from the Colorado Plateau garnet fragments discussed here, Fe–Mg zoning in garnets of peridotite nodules has been reported only in cases attributable to high-temperature metasomatism (e.g., Smith and Ehrenberg, 1984), not to cooling. Hence, we infer that olivine–garnet pairs in typical low-temperature nodules were not in Fe–Mg exchange disequilibrium due to mantle cooling, because Fe–

Mg zoning has not been reported in them. Our studies do not eliminate the possibility that recrystallization at low temperatures could destroy zoning and yet not produce equilibrium. In two of the Jagersfontein nodules garnet was not a primary phase but formed by reactions involving other minerals: cation partitioning between phases in these two samples is similar to that in rock J34, which has large, apparently primary garnet crystals, so equilibrium appears to have been maintained during recrystallization.

Though garnets should become zoned during cooling below 600°C or so in mantle environments in which the rate of conductive cooling is moderated by the thickness and heat production of overlying continental crust, cation distributions could freeze in without detectable zoning during faster cooling. Masses of garnet peridotite tectonically emplaced into the crust might retain Fe–Mg distributions from their mantle environments. Some of the zoning reported in phases in spinel peridotite nodules may reflect short-lived, local thermal events, such as magma intrusion, rather than the cooling of larger regions like that modelled here.

The size-composition dependence of olivine inclusions in garnet also characterizes disequilibrium due to cooling. The size dependence arises in the temperature range in which zoning originates, but the effect is easier to observe than the limited zones of iron enrichment about small inclusions. Moreover, it may be useful when the outer parts of garnet crystals have been destroyed during or after plucking from the mantle, as is commonly the case in diatreme nodules; strong zoning is present only in the outer 1 mm of the 3.5 mm radius garnets in our numerical experiments. The size-composition effect is different from that found by Ozawa (1983), in that he observed and calculated the effect in zoned spinel grains enclosed by olivine. Compositions of the spinel grains depended upon size because diffusion inwards from spinel perimeters was more effective in modifying the interiors of smaller grains than of larger ones. A similar size-composition dependence could be expected here for zoned garnet crystals in an appropriate size range. In contrast, the olivine inclusions remain homogeneous during cooling, but the amount of iron which is removed from any olivine inclusion depends upon the relative volume of garnet in effective communication with it, and hence upon the radius of the inclusion.

The identical Fe/Mg ratios in garnet in near contact with olivine, diopside, and orthopyroxene are consistent with the hypothesis that garnet in the Jagersfontein nodules was in Fe–Mg exchange equilibrium with pyroxene as well as with olivine. If Fe–Mg interdiffusion in clinopyroxene is much slower than in garnet, then pyroxene in contact with garnet might be zoned and the garnet might be homogeneous after cooling at suitable rates, as discussed by Lasaga (1983). No Fe–Mg zoning was observed in diopside in the Jagersfontein rocks, but no large diopside and garnet crystals were observed in mutual contact. Large orthopyroxene and garnet crystals are in contact in nodule J34, and the orthopyroxene crystals are homogeneous in Fe, Mg, Ca, and Al. The lack of zoning is evidence that orthopyroxene also continued to equilibrate until olivine-garnet temperatures of 700–800°C were reached in the Jagersfontein cooling history. In contrast, pyroxene inclusions in Colorado Plateau garnets are zoned in Fe, Mg, Ca, and Al, so garnet–olivine and garnet–pyroxene cation exchange may freeze in the same general P–T range in some mantle cooling histories.

The general accuracy of the olivine–garnet temperatures is supported by the consistency of the results from our numerical experiments with the temperatures calculated for the low-temperature pairs. Garnet is zoned in the Colorado Plateau pairs, with calculated temperatures near 550°C, and it is homogeneous in the Jagersfontein pairs, with values in the 700–800°C range. These temperatures are in accord with those considered appropriate by Tracy (1982) for the preservation or homogenization of garnet zoning in crustal metamorphic rocks. Carswell and Gibb (1980) showed that the olivine–garnet method generally yields lower temperatures for low-temperature peridotite than other methods, such as the two-pyroxene algorithm of Wells (1977). Since Lindsley (1983) has suggested that the Wells approach yields temperatures 100°C or more too high for metamorphic pyroxenes, the olivine-garnet temperatures may be more correct; they are broadly consistent with the recent pyroxene geothermometer of Kretz (1982) (Table 3). Even if the olivine–garnet temperatures are generally accurate, however, the problem posed by Harte and Freer (1982) and others remains—few other garnet peridotite nodules with equilibration temperatures below 800°C have been recognized in diatremes.

References

Bird P. R. (1979) Continental delamination and the Colorado Plateau. Journal of Geophysical Research, 84, 7561–7571.

Boyd, F. R. (1973) A pyroxene geotherm. Geochimica and Cosmochima Acta, 37, 2533–2546.

Buening, D. K. and Buseck, P. R. (1973) Fe–Mg lattice diffusion in olivine. Journal of Geophysical Research, 78, 6852–6862.

Carswell, D. A. and Gibb, F. G. F. (1980) Geothermometry of garnet lherzolite nodules with special reference to those from the kimberlites of northern Lesotho. Contributions to Mineralogy and Petrology, 74, 403–416.

Cygan, R. T. and Lasaga, A. C. (1983) Self-diffusion of magnesium in garnet at 750–900°C. Geological Society of America Abstracts with Programs, 15, 552.

Duckworth, S. and Freer, R. (1981) Cation diffusion studies in garnet–garnet and garnet–pyroxene couples at high tempera-

tures and pressures. In Ford, C. E., Ed. Progress in Experimental Petrology, The Natural Environment Research Council Publications Series D, 18, p. 36–39. Eaton Press, Wallasey, G. B.

Ellis, D. J. and Green, D. H. (1979) An experimental study of the effect of Ca upon garnet–clinopyroxene Fe–Mg exchange equilibria. Contributions to Mineralogy and Petrology, 71, 13–22.

Elphick, S. C., Ganguly, J., and Loomis, T. P. (1981) Experimental study of Fe–Mg interdiffusion in aluminumsilicate garnet. Transactions American Geophysical Union (EOS) 62, 411.

Finnerty, A. A. and Boyd, F. R. (1984) Evaluation of thermobarometers for garnet peridotites. Geochimica et Cosmochimica Acts, 48, 15–27.

Freer, R. (1981) Diffusion in silicate minerals and glasses: a data digest and guide to the literature. Contributions to Mineralogy and Petrology, 76, 440–454.

Harte, B. and Freer, R. (1982) Diffusion data and their bearing on the interpretation of mantle nodules and the evolution of the mantle lithosphere. Terra Cognita, 2, 273–275.

Harte, B. and Gurney, J. (1982) Compositional and textural features of peridotite nodules from the Jagersfontein kimberlite pipe, South Africa. Terra Cognita, 2, 256–257.

Harte, B., Jackson, P. M., and Macintyre, R. M. (1981) Age of mineral equilibria in granulite facies nodules from kimberlite. Nature, 291, 147–148.

Hofmann, A. W. and Hart, S. R. (1978) An assessment of local and regional isotopic equilibrium in the mantle. Earth and Planetary Science Letters, 38, 44–62.

Hunter, W. C. and Smith, D. (1981) Garnet peridotite from Colorado Plateau ultramafic diatremes: hydrates, carbonates, and comparative geothermometry. Contributions to Mineralogy and Petrology, 76, 312–320.

Kawasaki, T. (1979) Thermodynamic analysis on the Fe–Mg exchange equilibrium between olivine and garnet: an application to the estimation of P–T relations of ultramafic rocks. Journal of the Japanese Association of Mineralogists, Petrologists, and Economic Geologists, 74, 395–405.

Kretz, R. (1982) Transfer and exchange equilibria in a portion of the pyroxene quadrilateral as deduced from natural and experimental data. Geochimica et Cosmochimica Acta, 46, 411–421.

Lasaga, A. C. (1983) Geospeedometry: an extension of geothermometry. In Saxena, S. K., Ed., Kinetics and Equilibrium in Mineral Reactions, p. 81–114. Springer-Verlag, New York.

Lasaga, A. C., Richardson, S. M. and Holland, H. D. (1977) The mathematics of cation diffusion and exchange between silicate minerals during retrograde metamorphism. In Saxena, S. K. and Bhattacharji, S., Eds. Energetics of Geological Processes, p. 353–388. Springer-Verlag, New York.

Lindsley, D. H. (1983) Pyroxene thermometry. American Mineralogist, 68, 477–493.

Lindsley, D. H. and Andersen, D. J. (1983) A two-pyroxene thermometer. Proceedings of the Thirteenth Lunar and Planetary Science Conference, Part 2. Journal of Geophysical Research, 88, Supplement, A887–A906.

McGetchin, T. R. and Silver, L. T. (1970) Compositional relations in minerals from kimberlite and related rocks in the Moses Rock dike, San Juan County, Utah. American Mineralogist, 55, 1738–1771.

Misener, D. J. (1974) Cationic diffusion in olivine to 1400°C and 35 kbar. In Hoffman, A. W., Giletti, B. J., Yoder, H. S., and R. A. Yund, Eds., Geochemical Transport and Kinetics, p.

117–129, Carnegie Institute of Washington Publication V. 634, Washington, D. C.

Nixon, P. H. and Boyd, F. R. (1973) Petrogenesis of the granular and sheared ultrabasic nodule suite in kimberlites. In P. H. Nixon, Ed., Lesotho Kimberlites, p. 48–56. Cape and Transvaal Printers Ltd., Cape Town.

Oldenburg, D. W. (1975) A physical model for the creation of the lithosphere. Geophysical Journal of the Royal Astronomical Society, 43, 425–451.

O'Neill, H. St.C. (1981) The transition between spinel lherzolite and garnet lherzolite and its use as a geobarometer. Contributions to Mineralogy and Petrology, 77, 185–194.

O'Neill, H. St.C. and Wood, B. J. (1979) An empirical study of Fe–Mg partitioning between olivine and garnet and its calibration as a geothermometer. Contributions to Mineralogy and Petrology, 70, 59–70.

Onorato, P. I. K., Hopper, R. W., Yinnan, H., Uhlmann, D. R., Taylor, L. A., Garrison, J. R., and Hunter, R. (1981) Solute partitioning under continuous cooling conditions as a cooling rate indicator. Journal of Geophysical Research, 86, 9511–9518.

Ozawa, K. (1983) Evaluation of olivine–spinel geothermometry as an indicator of thermal history for peridotites. Contributions to Mineralogy and Petrology, 82, 52–65.

Pollack, H. N. and Chapman, D. S. (1977) On the regional variation of heat flow, geotherms, and lithospheric thickness. Tectonophysics, 38, 279–296.

Sanford, R. F. (1982) Three FORTRAN programs for finite-difference solutions to binary diffusion in one and two phases with composition- and time-dependent diffusion coefficients. Computers and Geosciences, 8, 235–263.

Smith, D. and Ehrenberg, S. N. (1984) Zoned minerals in garnet peridotite nodules from the Colorado Plateau: implications for mantle metasomatism and kinetics. Contributions to Mineralogy and Petrology, 86, 274–285.

Smith, D. and Levy, S. (1976) Petrology of the Green Knobs diatreme and implications for the upper mantle below the Colorado Plateau. Earth and Planetary Science Letters, 29, 107–125.

Tracy, R. J. (1982) Compositional zoning and inclusions in metamorphic minerals. In Ferry, J. M., Ed., Reviews in Mineralogy, V. 10, Characterization of metamorphism through mineral equilibria, p. 355–397. Mineralogical Society of America, Washington, D. C.

Wells, P. R. A. (1977) Pyroxene thermometry in simple and complex systems. Contributions to Mineralogy and Petrology, 62, 129–139.

Wilson, A. (1982) The geology of the great 'dyke', Zimbabwe: the ultramafic rocks. Journal of Petrology, 23, 240–292.

Wilson, C. R. and Smith, D. (1984a) Cooling rate estimates from mineral zonation: resolving power and applications. In J. Kornprobst, Ed., Proceedings of the Third International Kimberlite Conference, 2, 265–275.

Wilson, C. R. and Smith, D. (1984b) Cooling rate estimates from mineral zonation: resolving power and applications: Appendix. Kimberlite III Documents, Annales de Universite de Clermont-Ferrand, 73, 179–182.

Wood, B. J. (1974) The solubility of alumina in orthopyroxene coexisting with garnet. Contributions to Mineralogy and Petrology, 46, 1–15.

Appendix
Numerical Solution of the Diffusion Equation

The diffusion equation in radial coordinates is given by (1). It is assumed that there is no dependence of diffusivity D on concentration u, hence no dependence of D on spatial variable x within each phase. Let the subscript i refer to the variable x, so that $x = i\Delta x$, and the subscript m refer to the t variable so that $t = m\Delta t$. Following conventional procedures, replace the continuous time function by its discrete equivalent in equation (2). The partial derivatives become differences as shown in equations (3) and (4), where a two point difference is used for the first derivative of u to keep it centered about the value "i". The backward time difference is used to approximate the time derivative as shown in equation (5).

Defining the constants A, B and C (equation 6), the difference equation governing diffusion in a homogeneous material is given in equation (7). The objective is to solve for u as time advances. By representing the spatial dependence of concentrations with vectors $\vec{u}$, the discretized diffusion equations can then be written as a set of simultaneous linear equations (equation 8), where P is a tri-diagonal matrix, and the subscript i is no longer needed with the matrix - vector notation. The ith row (equation 10) has 3 non-zero terms, centered with the diagonal; while the first and last row (equations 9 and 11) are determined by the condition that there is no flux, hence no concentration gradient. At interior boundaries there may be discontinuities in both diffusion coefficients and concentration. Denote the two phases by subscripts a and b so that D_a and D_b are diffusion coefficients and R is the ratio of the concentration of phase b to that of phase a at the boundary, as in equation (12). The flux, F, across the boundary must be continuous. Using a two point difference formula, F at the boundary is expressed by equation (13). To eliminate the need to specify both $u_{a_{i+1,m}}$ and $u_{b_{i+1,m}}$ one can solve for them in terms of F, substitute into the diffusion equations for $u_{a_{i,m}}$ and $u_{b_{i,m}}$, and solve each for F; then, one can equate them to obtain a single equation, using $Ru_{b_{i,m}}$ in place of $u_{a_{i,m}}$ for the boundary point.

The results of these operations can be expressed by dropping the subscripts a and b on the concentration u since there is no longer any overlap, as in equation (14). Finally, doing the backward time difference and rearranging, the rows of the matrices for the boundary location i become as in equations (15) and (16).

If concentration u is expressed in units of moles/m^3, then the flux continuity across the boundary is correctly accounted for by these results. However, it may be convenient to use a normalized variable instead of absolute concentration. If the normalizing constant for phase a is C_a, and for phase b is C_b, then the ith + 1 row is as above except that R is now the ratio of the normalized variables at the boundary. The ith row of the P matrix is given in equation (17).

(1) $\quad \dfrac{\partial u}{\partial t} = D\left[\dfrac{2}{x}\dfrac{\partial u}{\partial x} + \dfrac{\partial^2 u}{\partial x^2}\right]$

(2) $\quad u(x,t) \longrightarrow u_{i,m}$

(3) $\quad \dfrac{\partial u}{\partial x} \longrightarrow \dfrac{u_{i+1,m} - u_{i-1,m}}{2\Delta x}$

(4) $\quad \dfrac{\partial^2 u}{\partial x^2} \longrightarrow \dfrac{u_{i+1,m} - 2u_{i,m} + u_{i-1,m}}{\Delta x^2}$

(5) $\quad \dfrac{\partial u}{\partial t} \approx \dfrac{u_{i,m} - u_{i,m-1}}{\Delta t}$

(6) $\quad C = \dfrac{D\Delta t}{\Delta x^2}, \quad A = \dfrac{1}{1+\frac{1}{i}} \quad \text{and} \quad B = \dfrac{1}{1-\frac{1}{i}}$

(7) $\quad u_{i,m} - u_{i,m-1} = C\left[\dfrac{1}{A}u_{i+1,m} - 2u_{i,m} + \dfrac{1}{B}u_{i-1,m}\right]$

(8) $\quad P\vec{u}_m = \vec{u}_{m-1}$

(9) $\quad \left[(1+2C), -2C, 0, 0, \ldots\right]$

(10) $\quad \left[\ldots, 0, \dfrac{-C}{B}, 1+2C, \dfrac{-C}{A}, 0, \ldots\right]$

(11) $\quad \left[\ldots, 0, -2C, 1+2C\right]$

(12) $\quad u_{b_{i,m}} = Ru_{a_{i,m}}$

(13) $\quad F = D_a\left[\dfrac{u_{a_{i+1}} - u_{a_{i-1}}}{2\Delta x}\right] = D_b\left[\dfrac{u_{b_{i+1}} - u_{b_{i-1}}}{2\Delta x}\right]$

(14) $\quad \dfrac{\partial u_i}{\partial t} = \dfrac{2D_a}{\Delta x^2(A+RB)}\left[\dfrac{D_b}{D_a}Bu_{i+1} - (AD_a + RBD_b)\dfrac{u_i}{D_a} + Au_{i-1}\right]$

(15) i + 1: $\left[\ldots, 0,0, -ACR\dfrac{D_b}{D_a}, \; 1+2C\dfrac{D_b}{D_a}, \; -\left(1+A\left(1-\frac{1}{B}\right)\right)C\dfrac{D_b}{D_a}, 0,0, \ldots\right]$

(16) i: $\left[\ldots,0,0, \dfrac{-2CA}{(A+RB)}, \; 1+\dfrac{2C}{(A+RB)}(A+RB\dfrac{D_b}{D_a}), \; \dfrac{-2CB}{(A+RB)}\cdot\dfrac{D_b}{D_a}, 0,0,\ldots\right]$

(17) $\left[\ldots,0,0, \dfrac{-2CA}{(A+RB\frac{C_b}{C_a})}, \; 1+\dfrac{2C}{(A+RB\frac{C_b}{C_a})}\cdot(A+RBC\dfrac{C_b}{C_a}\dfrac{D_b}{D_a}), \right.$
$\left. \dfrac{-2CB}{(A+RB\frac{C_b}{C_a})}\cdot\dfrac{D_b}{D_a}\cdot\dfrac{C_b}{C_a}, 0,0,\ldots\right]$